photonics

MDPI

Article

Dissimilar Laser Beam Welding of Titanium to Stainless Steel Using Pure Niobium as Filler Material in Lap Joint Configuration

Michael Wiegand [1,*], Alexander Kimm [1], Niklas Sommer [1], Linda Marks [2], Martin Kahlmeyer [1] and Stefan Böhm [1]

[1] Department for Cutting and Joining Manufacturing Processes, Institute for Production Technologies and Logistics, University of Kassel, Kurt-Wolters-Str. 3, 34125 Kassel, Germany; n.sommer@uni-kassel.de (N.S.); m.kahlmeyer@uni-kassel.de (M.K.); s.boehm@uni-kassel.de (S.B.)

[2] NMI Natural and Medical Sciences, University of Tübingen, Markwiesenstr. 55, 72770 Reutlingen, Germany

* Correspondence: m.wiegand@uni-kassel.de; Tel.: +49-561-804-3863

Abstract: In the present investigation, commercially pure titanium is welded to AISI 316L stainless steel by intermixing niobium as filler material in a lap joint configuration. For this purpose, a pulsed Nd:YAG laser with various pulse durations and pulse peak powers is employed to obtain different mixing conditions for the materials. It will be demonstrated that, despite the implementation of the filler material, the weld seams are characterized by a high affinity for cracking, which in turn can be attributed to the formation of hard intermetallic compounds. Nevertheless, utilization of optimized process parameters can yield crack-free specimens in a reproducible manner through equable intermixing of otherwise critical alloy elements. Lap-shear forces of up to 140 N can be achieved with a single weld seam measuring 2.5 mm in length. By increasing the joint area with four adjacent weld seams, maximum loads up to 320 N are attained, thus exceeding the yield strength of the applied stainless steel. Considering the biocompatibility of the niobium filler material used, this work provides the foundation for this dissimilar material combination to be implemented in future medical technology applications.

Keywords: pulsed laser beam welding; dissimilar welding; medical technology; intermetallic compounds

Citation: Wiegand, M.; Kimm, A.; Sommer, N.; Marks, L.; Kahlmeyer, M.; Böhm, S. Dissimilar Laser Beam Welding of Titanium to Stainless Steel Using Pure Niobium as Filler Material in Lap Joint Configuration. *Photonics* **2023**, *10*, 1063. https://doi.org/10.3390/photonics10091063

Received: 25 August 2023
Revised: 16 September 2023
Accepted: 19 September 2023
Published: 20 September 2023

1. Introduction

Dissimilar welded joints have the potential to combine the individual properties of different metals and, thus, generate various functional and economic advantages. In particular, hybrid parts made of commercially pure titanium (cp-Ti) and stainless steel are of high relevance in manifold industrial sectors, for example, the chemical, energy, and medical technology industries [1,2]. However, dissimilar fusion welding of cp-Ti to stainless steel is limited by thermophysical and chemical incompatibilities [1,3]. Based on the Fe-Ti phase diagram, it can be deduced that fusion welding of cp-Ti to iron-based alloys is restricted by very low solubility in the solid state as well as the formation of the intermetallic compounds (IMC) FeTi and Fe_2Ti [4]. These IMCs are characterized by extreme hardness values of up to 1000 HV and consequently impair the weldability and mechanical properties of fusion-welded joints substantially [1]. By using austenitic stainless steels with a high chromium and nickel content, other IMCs can be formed, e.g., $TiCr_2$, Ti_2Ni, and $Ti_5Fe_{17}Cr_5$, leading to an even more complex and generally unfavorable microstructure [1]. Further limitations in dissimilar welding arise from deviating melting temperatures, thermal conductivities, and thermal expansions of the materials, resulting in considerably increased stress conditions during cooling and the emergence of residual stresses [1,5,6].

Previous studies on autogenous beam welding of Ti to stainless steel have consequently achieved comparatively poor joint properties [3,7–10]. A promising approach was to apply a beam offset to one of the joining partners in order to reduce intermixing of the materials and, thus, the formation of critical IMCs [3,10]. Nevertheless, despite the adjusted parameters, maximum average tensile strengths of only 174 MPa were achieved in butt joint configuration [10]. In contrast, it was found that the chemical compatibility of the joint can be substantially increased using filler materials. Accordingly, recent investigations have demonstrated that the application of copper [9,11], vanadium [9,12,13], or nickel [9] as filler materials significantly enhances the weldability and mechanical performance of Ti/stainless steel dissimilar joints. However, regardless of the applied filler material, IMC formation cannot be fully prevented, and the weld metal remains the weak point of the welded parts. As a result, multiple groups of authors have tested multilayer configurations such as Nb/Cu [12,14,15], Nb/Ni [16], and Ta/Va/Fe [17] to further increase the chemical compatibility of the respective weld seams. Tensile strengths of up to 623 MPa with fracture in the unmelted vanadium were achieved using the latter combination [17], therefore confirming the effectiveness of using filler materials in conjunction with beam welding processes. Nevertheless, the aforementioned material combinations do not exclusively involve biocompatible materials and are consequently unsuitable for medical technology applications. In a recent study by Wiegand et al. [2], pure Nb was identified as a promising interlayer material for dissimilar welding of cp-Ti to stainless steel. By micro-electron beam welding, it was possible to achieve tensile strengths of up to 394 MPa in butt joint configuration. Owing to the biocompatible nature of Nb, this opens up new possibilities for dissimilar welding in medical applications.

The present investigation seeks to build on this study and addresses the intermixing of a Nb foil into a cp-Ti/Nb/316L dissimilar weld in a lap joint configuration. Complementary to the study by Wiegand et al. [2], in which the two base materials were completely separated by the filler material, the study at hand serves to evaluate the intermixing of the materials and the influence on the weldability and mechanical properties of the joints. Furthermore, the consideration of the lap joint and the utilization of a pulsed laser beam system can potentially generate further opportunities for a transfer into current medical technology applications. The welding process is ideally suited for the joining of small medical parts, as minimal weld pool sizes and heat-affected zones can be realized through precise parameter control [18]. In addition, this also allows to reduce the adverse effects of thermophysical incompatibilities of different materials, making pulsed laser beam welding very promising for fusion welding of critical material combinations [19].

Different pulse durations and pulse peak powers are applied to control the welding depth into the substrate sheet as well as the time for intermixing processes to tailor the chemical composition of the respective weld metal. The weld seams are analyzed regarding their weld penetration depth and defect formation using optical light microscopy. Selected samples are subsequently characterized by means of energy-dispersive X-ray spectroscopy (EDS) with respect to the elemental distribution in the weld metal. In order to correlate these results with the resulting hardness profiles as well as to detect critical weld seam areas that correspond to pronounced IMC formation, micro-hardness measurements are conducted. Finally, tensile tests are performed on the most promising parameter set to evaluate the mechanical resistance of the weld seams. The results demonstrate the effectiveness of targeted process and parameter optimization in pulsed laser beam welding and prove that the material combination cp-Ti/Nb/316L can be welded crack-free in a reproducible manner when intermixed in a lap joint configuration.

2. Materials and Methods

Thin sheet geometries measuring 12.5 × 25 × 0.25 mm^3 were used as base materials. As filler material, a Nb-foil with a thickness of 0.1 mm was inserted between both base

materials in a lap joint configuration (see Figure 1). All geometries were produced by electrical discharge machining (EDM). Table 1 lists selected thermophysical and mechanical properties of the applied materials.

Table 1. Selected thermophysical and mechanical properties of the respective materials used in this investigation. All values are given for a temperature of 20 °C (Adapted from [20–22]). The mechanical properties (*) are derived from tensile tests on the unwelded sheet materials.

Material	Melting Point [°C]	Ultimate Tensile Strength * [MPa]	Elongation at Break * [%]	Thermal Conductivity [$Wm^{-1}K^{-1}$]	Coefficient of Thermal Expansion [$10^{-6}\,K^{-1}$]
cp-Titanium (grade 4)	1660	~679	~23	18	8.6
316L (X2CrNiMo17-12-2, annealed)	~1450	~656	~44	15	16
Niobium (purity 99.9%)	2468	~254	~42	52	7.1

The welding tests were performed on a 1064 nm pulsed Nd:YAG laser SLS 200 CL 8 (Coherent Switzerland AG, formerly ROFIN-LASAG AG, Belp, Switzerland) featuring a near-Gaussian intensity distribution and a beam diameter of approximately 38 µm. The welding system offers a maximum laser output power of 1 kW and the option to perform free-form pulse-shaping. The applied process parameters are summarized in Table 2. In order to achieve varying welding depths, the pulse peak power was increased in increments of 25 W, resulting in a total of 5 weld seams for each pulse duration. In addition, a customized pulse shape was implemented. Hence, the power was continuously reduced within the individual pulses to provide more homogeneous cooling conditions. For the specimens welded with a pulse duration of 1 ms, a reduction of the pulse interval to 0.05 mm was necessary to provide sufficient overlapping of the comparatively narrower weld metal. This was implemented with a slower traverse speed of 0.15 mm/s. The beam was focused on the surface of the top sheet.

Table 2. Overview of applied welding parameters.

Pulse Duration [ms]	Pulse Peak Power [W]	Traverse Speed [mm/s]	Pulse Frequency [Hz]	Pulse interval [mm]
1	700–800	0.15	3	0.05
3	400–500	0.3		0.1
7	300–400	0.3		0.1
10	250–350	0.3		0.1

The welding tests were carried out using 316L as the top sheet, cp-Ti as the substrate sheet, and vice versa. To ensure virtually gap-free positioning, the specimens were clamped in a special fixture. Furthermore, the welding processes were conducted using argon shielding gas (99.998% purity). To obtain optimal protection of the highly reactive materials, the welding area was covered with a slow flow rate of 6 L/min for a minimum of 30 s prior to the start of the welding processes. The experimental setup is visualized in Figure 1a, and the welding configuration is schematically illustrated in Figure 1b.

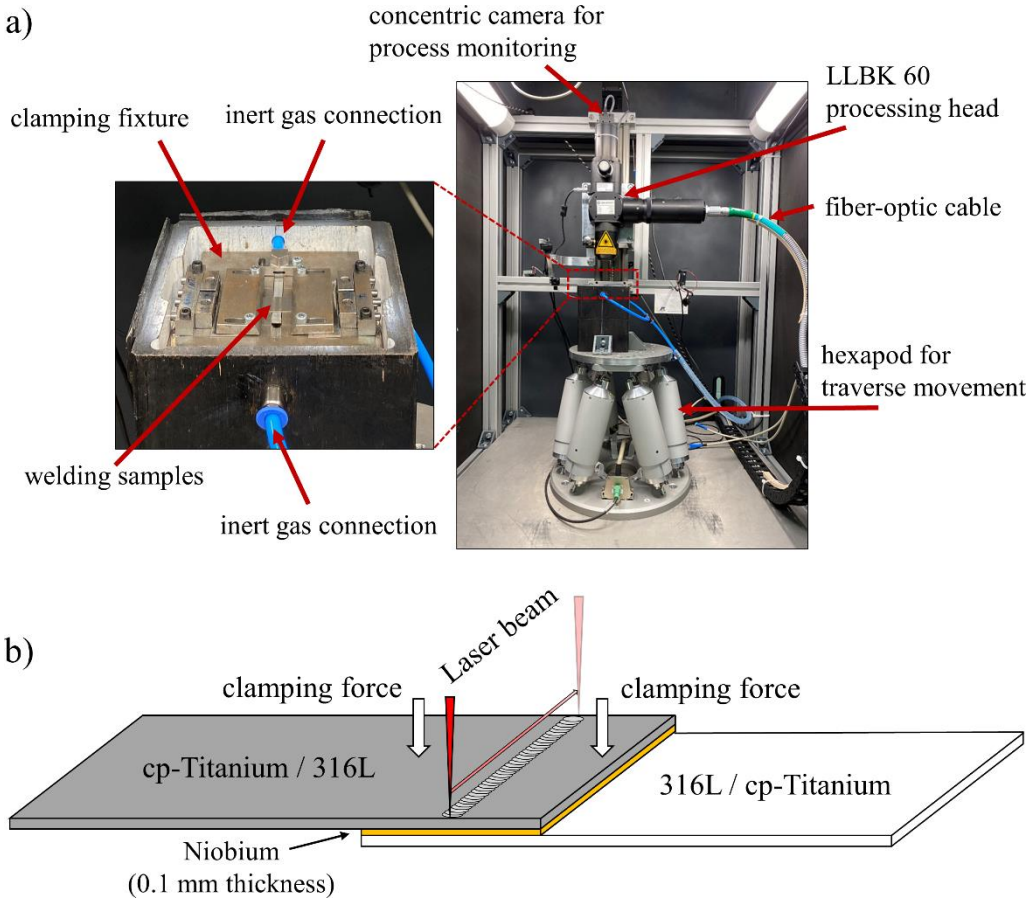

Figure 1. (**a**) Photographic images depicting the experimental setup of the welding process. During the welding operations, the housing of the clamping fixture was covered outside the beam path to ensure uniform shielding gas coverage. (**b**) Schematic illustration introducing the welding configuration.

The welded samples were analyzed by means of optical light microscopy (DM2700, Leica Microsystems GmbH, Wetzlar, Germany). For this purpose, the specimens were ground and subsequently polished using a diamond suspension with a 0.1 µm grit size. The etchants used were V2A-etchant (HNO_3 and HCl, 60 s at 60 °C) to highlight the microstructure of 316L and a hydrofluoric acid-free etching solution according to Keller (HCl, HNO_3, and NaF, 120 s at room temperature) to highlight the cp-Ti structure. The chemical distribution in the weld seams was characterized by means of scanning electron microscopy (SEM, Zeiss REM Ultra Plus, Carl Zeiss AG, Oberkochen, Germany) operated at an acceleration voltage of 15 kV using EDS (Bruker XFlash 6160, Bruker Corporation, MA, USA). Micro-hardness measurements were performed using an automated hardness-testing machine (KB30, KB Prüftechnik GmbH, Hochdorf-Assenheim, Germany). Shear tensile tests were conducted on a universal tensile-testing machine (Z100, ZwieckRoell AG, Ulm, Germany) in accordance with DIN EN ISO 12996 using three identically manufactured specimens. The samples were extracted from the welded parts using EDM and measured 2.5 mm in width.

3. Results and Discussion

3.1. 316 L as Top Sheet/cp-Ti as Substrate Sheet

The welding tests performed with 316L as the top sheet and cp-Ti as the substrate sheet were invariably characterized by pronounced solidification cracking longitudinal to the welding direction. Despite the high variation of parameters, no corresponding weld

seam was free of defects. As can be derived from the micro-hardness mapping of an exemplary sample in Figure 2a, the cracked specimens are characterized by extreme hardness values exceeding 1000 HV across the weld metal. These values correspond very well to the findings of previous studies on autogenous beam welding of Ti to stainless steel and indicate a pronounced formation of highly critical Fe_2Ti IMC [1,3]. Consequently, the high affinity for solidification cracking and the associated poor weldability can ultimately be attributed to the presence of IMCs formed by the extensive mixing of 316L and cp-Ti.

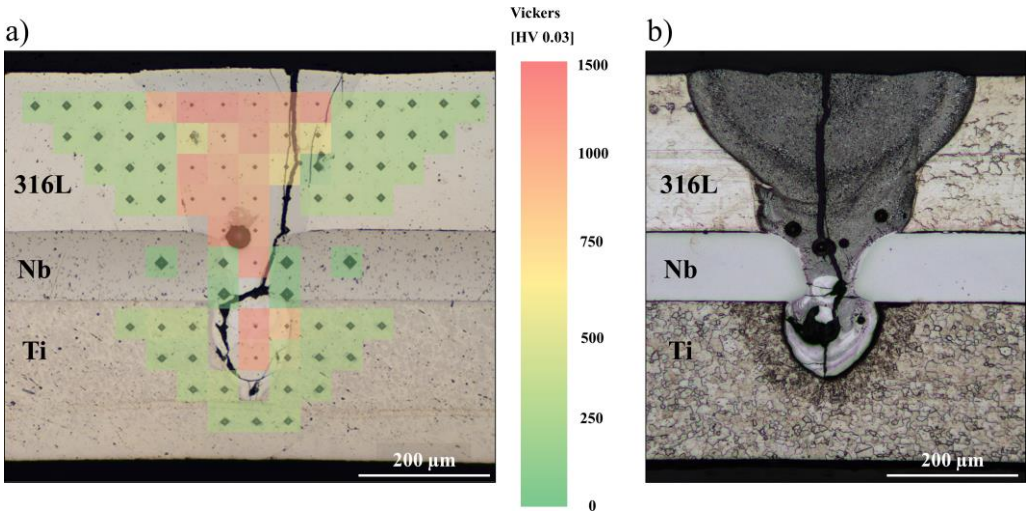

Figure 2. (**a**) Micro-hardness mapping of an exemplary specimen with 316L as the top sheet and cp-Ti as the substrate sheet (3 ms, 500 W); (**b**) Etched cross-section of another specimen (10 ms, 350 W).

Another observation that can be derived from Figure 2 is the concise shape of the weld metal, which is also reflected in the course of the hardness profile. As the etched cross-section of another representative sample in Figure 2b shows in greater detail, the weld metal is narrowed as the weld penetration depth increases and eventually constricts considerably at the level of the filler metal. Similar weld metal shapes were reported by Ge et al. [23] on a comparable material arrangement in a NiTi/Nb/Ti_2AlNb laser-welded lap joint. This observation can be attributed to the substantially higher melting temperature and thermal conductivity of the Nb filler material compared to the base materials, as shown in Table 1. From the decreasing weld seam width, it can be deduced that the proportion of the intermixed alloying elements of 316L is inevitably substantially higher than that of the filler and substrate materials for the particular joint. According to the findings of Mannucci et al. [10], limiting the intermixing of stainless steel in dissimilar welding with titanium is expedient in order to reduce critical IMC formation and to obtain improved weldability and mechanical properties. In consideration of the observed severe crack formation and the apparently inadequate weldability with the given material arrangement due to the dominating proportion of 316L in the weld metal, no further investigations were carried out in this orientation.

3.2. cp-Ti as Top Sheet/316L as Substrate Sheet

By applying cp-Ti as the top sheet and 316L as the substrate sheet, the weldments can be expected to have a significantly reduced proportion of intermixed 316L compared to the welding tests of the previous section. Nevertheless, despite the adjusted material arrangement, the welding tests with pulse durations of 1 ms, 3 ms, and 7 ms are equally characterized by major crack formation in the longitudinal direction of the welding trajectory. Thus, the weldability of the dissimilar joint remains poor, and the mixing of the materials further promotes the formation of solidification cracks due to their chemical incompatibility. As exemplified by the welding tests conducted with a pulse duration of 7 ms in Figure 3, the defect formation is strongly dependent on the welding penetration depth in

the 316L sheet. While the longitudinal crack in the weld seam generated with 325 W pulse peak power does not extend over the full length of the bead, the crack development increases significantly with higher energy input. This confirms the previously established conclusion that the proportion of intermixed stainless steel in the weld metal must be minimized in order to generate low-defect joints.

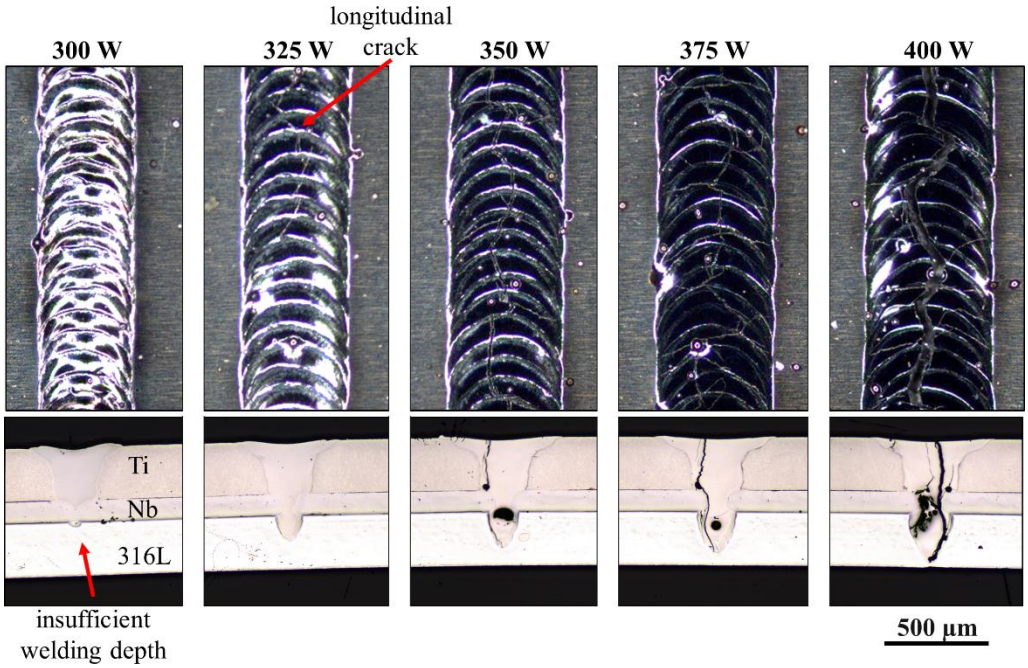

Figure 3. Weld seam surfaces and cross-sections of weld seams generated a pulse duration of 7 ms and pulse peak powers of 300 W to 400 W. Note that the differing colors of the weld seam surfaces are caused by deviating light reflections resulting from the varying topography of the weld metal.

However, despite the high affinity for solidification cracking of the investigated material combination, it was possible to identify a parameter set that not only generates defect-free weld seams in a reproducible manner but also achieves superior mechanical properties. Accordingly, the utilization of a comparatively long pulse duration of 10 ms can drastically reduce the general tendency for crack initiation.

Based on this finding, a significant impact of the parameters on the weldability of the joint can be deduced, which is further experimentally determined in the following by means of EDS analyses. In this context, an exemplary specimen exhibiting longitudinal cracking, which was welded with a pulse duration of 3 ms as well as a pulse peak power of 500 W, is characterized with respect to the elemental distribution, as shown in Figure 4. The investigation reveals severe mixing gradients regarding Ti and Fe across the height of the weld seams. Owing to the sheet arrangement, a higher concentration of Fe can be identified in the weld seam root. In the upper area of the weld seam, the proportion of Fe decreases and is further defined by an inhomogeneous distribution. Analogously, the proportion of Ti decreases in the region of the weld seam root. This observation can be explained by the comparatively short pulse duration of 3 ms in conjunction with the small beam diameter of the laser system, which leads to rapid solidification of the weld metal. As a result, intermixing processes have insufficient time to take effect.

Compared to Ti and Fe, Nb is distributed rather homogeneously in the weld metal, although to an apparently smaller amount. The comparatively low proportion in the weld metal can ultimately be attributed to the high melting temperature of the refractory metal mentioned previously and the associable, constricted weld geometry, resulting in a reduced volume of molten and intermixed Nb. Thus, it can be concluded that areas with a

high content of 316L will inevitably mix with a considerable amount of Ti, therefore increasing the risk of critical Fe_2Ti IMC formation. Finally, this explains the high affinity for cracking in weld seam root, where a highly concentrated Fe dispersion was detected.

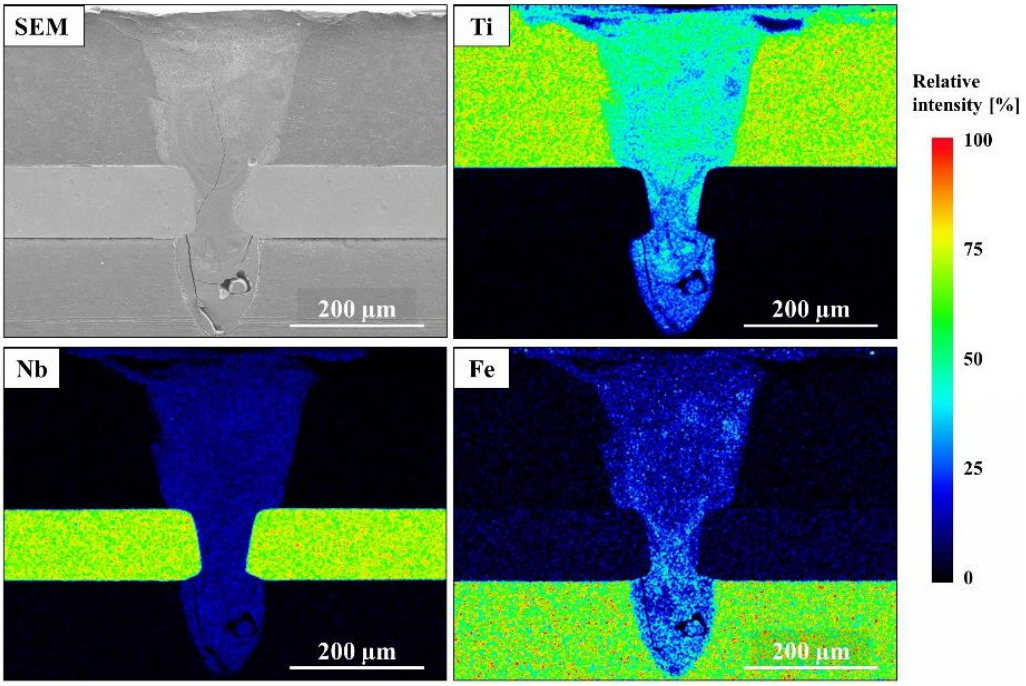

Figure 4. SEM image and corresponding EDS mappings of a representative sample (pulse duration 3 ms, pulse peak power 500 W) with longitudinal cracking visualizing the relative intensity distribution of Ti, Nb, and Fe in the weld metal.

In the following, an identical analysis of the relative material distribution in the weld metal is provided for a crack-free specimen welded with a pulse duration of 10 ms and a pulse peak power of 300 W. In comparison to the sample in Figure 4, the crack-free sample is characterized by a very homogenous material distribution of Fe, Ti, and Nb throughout the weld metal, as can be seen in Figure 5. Even in the area of the weld seam root, only minor mixing gradients can be identified along the fusion lines. Thus, it can be concluded that a prolongation of the pulse duration promotes a uniform chemical distribution of the base and filler materials. This can be explained by the increased interaction time between the beam and the material, leading to an extended residence time for the weld metal in the liquid phase. Consequently, intermixing processes have more time to occur, thus enabling the melt pool convection to promote an equable element distribution. Furthermore, the penetration depth in the substrate sheet is relatively low compared to the cracked sample in Figure 4, which ultimately results in a reduced proportion of intermixed 316L. This observation can be attributed to the reduced pulse peak power of 300 W. It should be noted at this point that increased laser powers again yielded solidification cracking, even at pulse durations of 10 ms, proving yet again that the amount of molten and intermixed 316L should be minimized (images not shown).

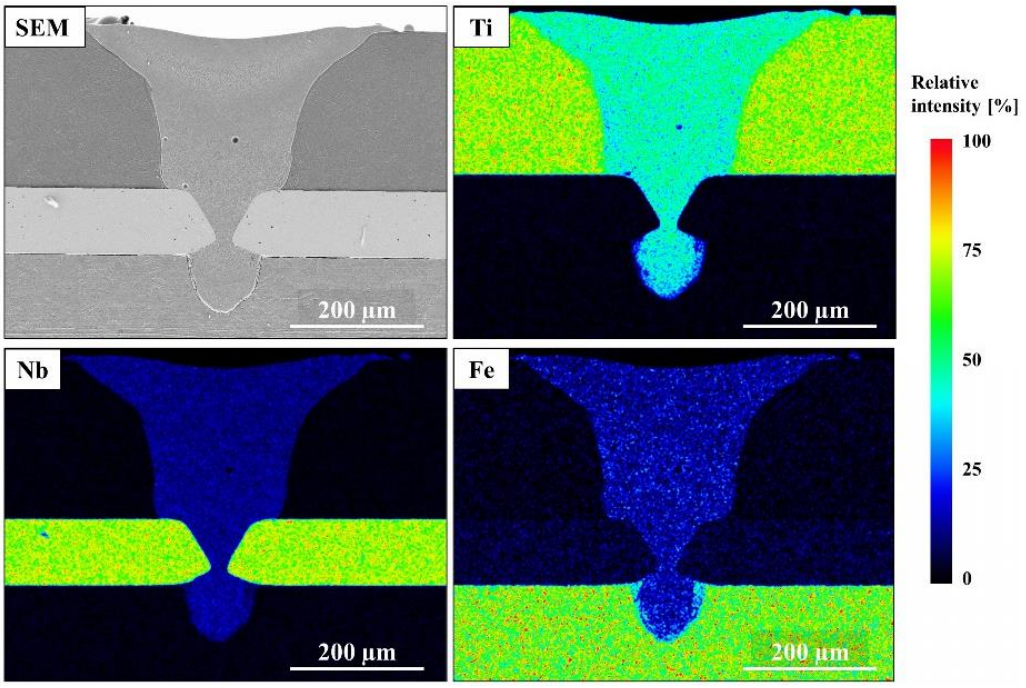

Figure 5. SEM image and associated EDS mappings of the crack-free parameter set (pulse duration 10 ms, pulse peak power 300 W) revealing the relative intensity distribution of Ti, Nb, and Fe in the weld metal.

In order to correlate the differing material distributions of the two samples from Figures 4 and 5 with their respective mechanical properties, subsequent micro-hardness mappings were performed. As shown in Figure 6a, the previously identified mixing gradients of Ti and Fe in the weld metal have a substantial impact on the resulting hardness of the joint. It can be seen that hardness values of more than 1000 HV exist in the bottom area of the weld seam, in which a distinct accumulation of Fe as well as an increased susceptibility to cracking had been identified previously. Analogously, in the upper section of the weld seam, the proportion of Fe is significantly lower, and, thus, the hardness declines to values between approximately 500 and 600 HV.

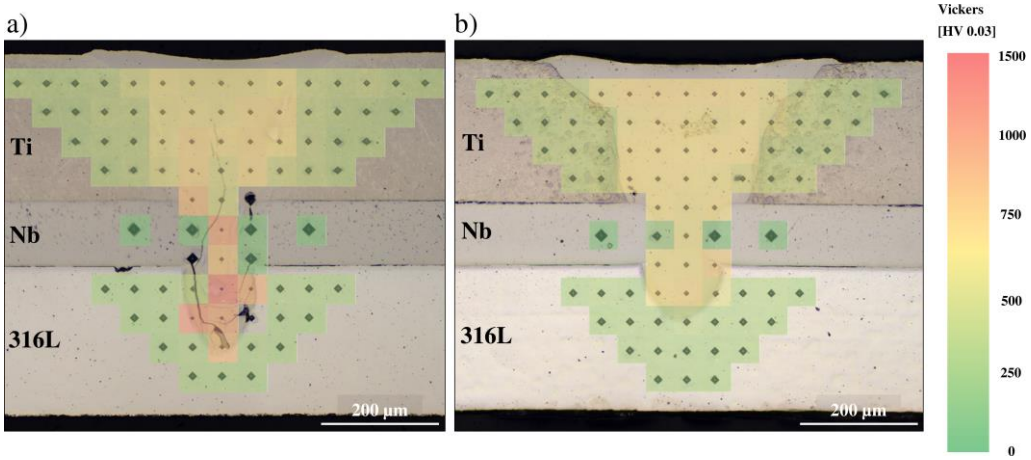

Figure 6. Micro-hardness mappings of samples welded with (**a**) 3 ms pulse duration and 500 W pulse peak power as well as (**b**) 10 ms pulse duration and 300 W pulse peak power.

As illustrated in Figure 6b, the hardness values of the crack-free sample welded with 10 ms pulse duration are distributed very uniformly across the weld metal. Compared to the sample welded with 3 ms pulse duration, the specimen also exhibits substantially

lower hardness values, averaging at approximately 520 HV in the weld metal. Although this still represents an increase in hardness compared to the base metals, the values are significantly lower than those of areas with high IMC concentration. The comparatively low penetration depth, the homogenous material distribution, and ultimately the intermixing of Nb apparently reduce the global formation of critical IMCs such as Fe_2Ti and, thus, substantially decrease the susceptibility to solidification cracking. In accordance with the findings of previous studies on dissimilar welding of titanium to stainless steel, the chemical composition of the weld metal therefore exerts a significant influence on the weldability of the joint and requires systematic parameter optimization in order to generate uncritical microstructural conditions.

In order to evaluate the mechanical performance of the crack-free parameter set, shear tensile tests were carried out. As can be derived from Figure 7a, the welded specimens, which measure a width of 2.5 mm, can withstand a lap-shear force of up to 140 N when welded with a single weld seam. It should be emphasized that the specimens always failed in the transition area between the niobium filler material and the 316L substrate sheet and, thus, along the smallest connection area of the joint. Based on this observation, additional shear tensile testing specimens with four adjacent weld seams were fabricated in order to increase the total connection area. By this approach, the bond strength was increased, reaching lap-shear forces of up to 320 N, which correspond to approximately 78% of the ultimate tensile strength of the applied 316L sheet with a given cross-sectional area of 2.5 × 0.25 mm^2. As can be seen in the associated lap-shear-force elongation diagram in Figure 7b, the yield strength of the 316L base material can be surpassed by the quadruple weld configuration. Consequently, these findings showcase the high potential to apply comparable weld configurations in industrial applications, e.g., parts in the medical technology sector.

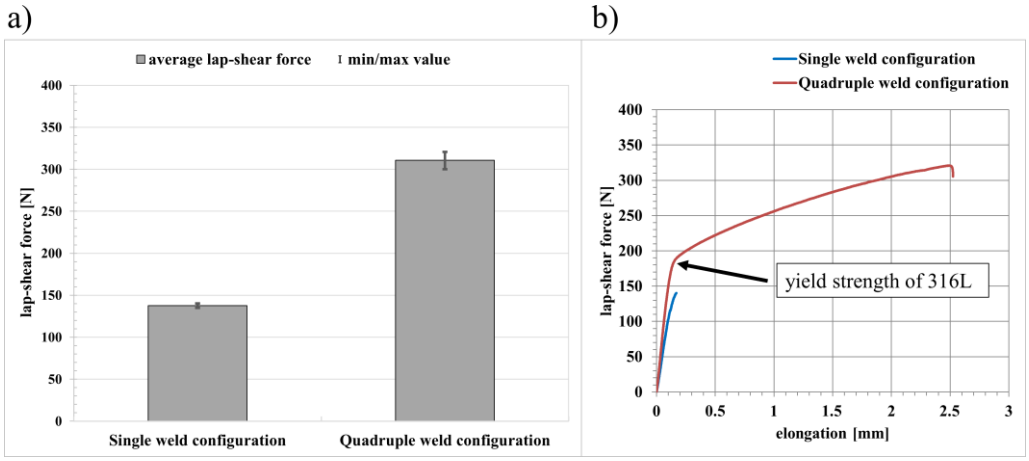

Figure 7. (**a**) Comparison of lap-shear force data obtained by the shear tensile tests for the crack-free single and quadruple weld configurations, generated with 10 ms pulse duration and 300 W pulse peak power. (**b**) Lap-shear-force elongation diagram of two representative specimens.

Figure 8a shows macroscopic images of a corresponding specimen in postmortem condition, i.e., after the shear tensile test. Based on the bottom view of the sample, it can be seen that the fracture occurs in the outermost weld metal in the direction of the tensile load applied to the 316L sheet. As can be seen in the associated cross-section, material separation occurs along the fusion line in the weld seam root, whereas the weld metal remains intact. Below the weld metal, a ductile fracture area also becomes apparent, eventually caused by the unmelted 316L base material. As was observed in Figure 5, minimally increased Fe concentrations are found in the range of the fusion line. This may result in a thin layer of pronounced IMC formation, thus initiating premature failure in the corresponding area. However, in order to fully understand the failure process, further analyses using in situ digital image correlation during shear testing as well as a subsequent fracture

surface analysis are required. These analyses form part of an ongoing study and will be the focus of an upcoming publication in the field.

The illustration in Figure 8b schematically visualizes the area of fracture in a cross-sectional view. Based on the recurring fracture along the outermost weld seam for each specimen, an uneven stress distribution can be deduced, which ultimately promotes premature failure. Future investigations should therefore also aim at further increasing the mechanical properties by specifically adapting the bonding area, for example, by generating weld seams longitudinally to the direction of the applied load.

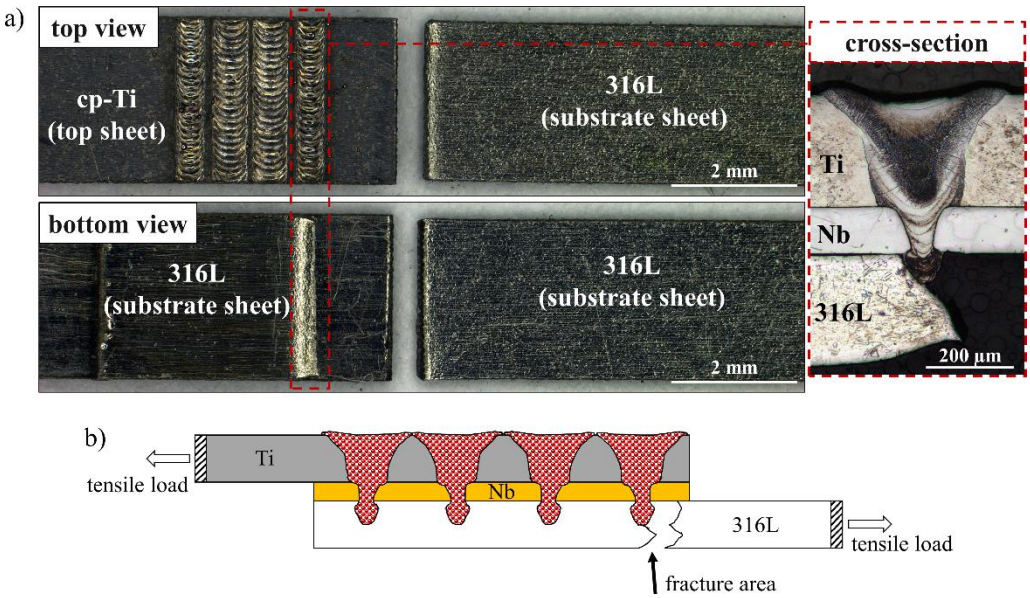

Figure 8. (**a**) Macroscopic images of a specimen with quadruple weld configuration, displaying the top and bottom view as well as the cross-sectional area of the fracture following shear tensile testing; (**b**) Schematic illustration of the specimen cross-section, highlighting the fracture area and introducing the fracture mode.

While the investigation at hand provides crucial information about the parametric influence of pulsed laser beam welding on the dissimilarly welded cp-Ti/Nb/316L lap joint, further microstructural investigations are needed in order to understand the complex solidification mechanisms and to precisely identify the resulting phases and IMCs. Moreover, additional adjustments should be made with regard to the proportion of intermixed Nb to better understand the influence of the filler metal on the microstructural evolution. For this purpose, different geometries of the filler material should be investigated, since this approach has also led to significant improvements of the joint properties in previous studies [24]. In addition to a change in the specimen geometry, adapted pulse-shaping should be considered to further control the weld metal geometry and the intermixing processes.

4. Conclusions

The investigation at hand demonstrates that dissimilar joints between cp-Ti and 316L can be welded crack-free with good mechanical properties by using Nb as filler material in lap joint configuration. However, weldability is significantly influenced by the applied process parameters, which consequently require systematic optimization to produce non-critical chemical compositions in the weld metal. The experimental results reveal that a limitation of the intermixed proportion of 316L as well as a homogeneous material distribution in the weld metal should be aimed for. In the case of the present investigation, this was achieved by a comparatively high pulse duration of 10 ms and a low welding depth into the 316L substrate sheet. Owing to the good mechanical resilience of the weld seams in conjunction with the biocompatibility of the filler material used, the results of this work

provide the foundation for this material combination to be used in future medical technology applications. Nevertheless, further studies should be performed to better understand the microstructural evolution of the dissimilar welded joint as well as to precisely identify the resulting phases and IMCs, respectively. Based on these analyses, the numerous process parameters of pulsed laser beam welding can be specifically adapted to potentially further improve the mechanical properties of the weldments and shall thus be the focus of future investigations.

Author Contributions: Conceptualization, M.W.; methodology, M.W., and A.K.; validation, S.B.; formal analysis, M.W., and A.K.; investigation, M.W., A.K., N.S., L.M., and M.K.; data curation, M.W.; writing—original draft preparation, M.W.; writing—review and editing, A.K., N.S., L.M., M.K., and S.B.; visualization, M.W.; supervision, S.B.; project administration, M.W.; funding acquisition, S.B. All authors have read and agreed to the published version of the manuscript.

Funding: The shown results were achieved in the project "Artfremdes Mikro-Strahlschweißen von Titan mit Nitinol und nichtrostenden Stählen zur Herstellung eines biokompatiblen Materialverbunds unter Verwendung von Zusatzwerkstoffen (MeTiWeld)" (reference IGF 21.601 N), which is supervised by the Forschungsvereinigung Schweißen und verwandte Verfahren e.V. of the German Welding Society and funded by the German Federation of Industrial Research Associations (AiF) by means of the Federal Ministry for Economic Affairs and Climate Action (BMWK) on the basis of a decision by the German Bundestag.

Institutional Review Board Statement: Not applicable.

Informed Consent Statement: Not applicable.

Data Availability Statement: The data underlying the results presented in this paper are not publicly available as they are part of an ongoing investigation.

Conflicts of Interest: The authors declare no conflict of interest.

References

1. Quazi, M.M.; Ishak, M.; Fazal, M.A.; Arslan, A.; Rubaiee, S.; Qaban, A.; Aiman, M.H.; Sultan, T.; Ali, M.M.; Manladan, S.M. Current research and development status of dissimilar materials laser welding of titanium and its alloys. *Opt. Laser Technol.* **2020**, *126*, 106090. https://doi.org/10.1016/j.optlastec.2020.106090.
2. Wiegand, M.; Marks, L.; Sommer, N.; Böhm, S. Dissimilar micro beam welding of titanium to Nitinol and stainless steel using biocompatible filler materials for medical applications. *Weld. World* **2023**, *67*, 77–88. https://doi.org/10.1007/s40194-022-01412-3.
3. Chen, S.; Zhang, M.; Huang, J.; Cui, C.; Zhang, H.; Zhao, X. Microstructures and mechanical property of laser butt welding of titanium alloy to stainless steel. *Mater. Des.* **2014**, *53*, 504–511. https://doi.org/10.1016/j.matdes.2013.07.044.
4. Cacciamani, G.; de Keyzer, J.; Ferro, R.; Klotz, U.E.; Lacaze, J.; Wollants, P. Critical evaluation of the Fe–Ni, Fe–Ti and Fe–Ni–Ti alloy systems. *Intermetallics* **2006**, *14*, 1312–1325. https://doi.org/10.1016/j.intermet.2005.11.028.
5. Datta, S.; Raza, M.S.; Kumar, S.; Saha, P. Exploring the possibility of dissimilar welding of NiTi to Ti using Yb-fiber laser. *Adv. Mater. Process. Technol.* **2018**, *4*, 614–625. https://doi.org/10.1080/2374068X.2018.1486533.
6. Shojaei Zoeram, A.; Akbari Mousavi, S. Laser welding of Ti–6Al–4V to Nitinol. *Mater. Des.* **2014**, *61*, 185–190. https://doi.org/10.1016/j.matdes.2014.04.078.
7. Satoh, G.; Yao, Y.L.; Qiu, C. Strength and microstructure of laser fusion-welded Ti–SS dissimilar material pair. *Int. J. Adv. Manuf. Technol.* **2013**, *66*, 469–479. https://doi.org/10.1007/s00170-012-4342-6.
8. Shanmugarajan, B.; Padmanabham, G. Fusion welding studies using laser on Ti–SS dissimilar combination. *Opt. Lasers Eng.* **2012**, *50*, 1621–1627. https://doi.org/10.1016/j.optlaseng.2012.05.008.
9. Wang, T.; Zhang, B.; Feng, J. Influences of different filler metals on electron beam welding of titanium alloy to stainless steel. *Trans. Nonferrous Met. Soc. China* **2014**, *24*, 108–114. https://doi.org/10.1016/S1003-6326(14)63034-X.
10. Mannucci, A.; Tomashchuk, I.; Mathieu, A.; Cicala, E.; Boucheron, T.; Bolot, R.; Lafaye, S. Direct laser welding of pure titanium to austenitic stainless steel. *Procedia CIRP* **2018**, *74*, 485–490. https://doi.org/10.1016/j.procir.2018.08.138.
11. Zhang, Y.; Sun, D.Q.; Gu, X.Y.; Liu, Y.J. Nd/YAG pulsed laser welding of TC4 titanium alloy to 301L stainless steel via pure copper interlayer. *Int. J. Adv. Manuf. Technol.* **2017**, *90*, 953–961. https://doi.org/10.1007/s00170-016-9453-z.
12. Mannucci, A.; Tomashchuk, I.; Mathieu, A.; Bolot, R.; Cicala, E.; Lafaye, S.; Roudeix, C. Use of pure vanadium and niobium/copper inserts for laser welding of titanium to stainless steel. *J. Adv. Join. Process.* **2020**, *1*, 100022. https://doi.org/10.1016/j.jajp.2020.100022.
13. Zhang, Y.; Zhou, J.; Sun, D.; Li, H. Two pass laser welding of TC4 Titanium alloy to 301L stainless steel via pure V interlayer. *J. Mater. Res. Technol.* **2020**, *9*, 1400–1404. https://doi.org/10.1016/j.jmrt.2019.11.066.

14. Fang, Y.; Jiang, X.; Song, T.; Mo, D.; Luo, Z. Pulsed laser welding of Ti-6Al-4V titanium alloy to AISI 316L stainless steel using Cu/Nb bilayer. *Mater. Lett.* **2019**, *244*, 163–166. https://doi.org/10.1016/j.matlet.2019.02.075.
15. Li, J.; Liu, Y.; Gao, Y.; Jin, P.; Sun, Q.; Feng, J. Benefits of interfacial regulation with interlayers in laser welding Ti6Al4V/316L steel. *Opt. Laser Technol.* **2020**, *125*, 106007. https://doi.org/10.1016/j.optlastec.2019.106007.
16. Zhang, Y.; Zhou, J.; Sun, D.; Li, H. Three-pass laser welding of Ti alloy-stainless steel using Nb and Ni interlayers. *J. Mater. Res. Technol.* **2020**, *9*, 1780–1784. https://doi.org/10.1016/j.jmrt.2019.12.009.
17. Zhang, Y.; Sun, D.Q.; Gu, X.Y.; Duan, Z.Z.; Li, H.M. Nd:YAG pulsed laser welding of TC4 Ti alloy to 301L stainless steel using Ta/V/Fe composite interlayer. *Mater. Lett.* **2018**, *212*, 54–57. https://doi.org/10.1016/j.matlet.2017.10.057.
18. Sommer, N.; Stredak, F.; Wiegand, M.; Böhm, S. Grain growth and precipitation behaviour of AISI 430 ferritic stainless steel subjected to pulsed laser beam welding using free-form pulse shaping. *Weld. World* **2023**, *67*, 51–62. https://doi.org/10.1007/s40194-022-01398-y.
19. Sun, Z.; Ion, J.C. Laser welding of dissimilar metal combinations. *J. Mater. Sci.* **1995**, *30*, 4205–4214. https://doi.org/10.1007/BF00361499.
20. METALCOR GmbH. Datenblatt: Titan-Grade 4 (3.7065). Available online: http://www.metalcor.de/datenblatt/124/ (accessed on 22 August 2023).
21. Deutsche Edelstahlwerke GmbH. Werkstoffdatenblatt 1.4404. Available online: https://www.dew-stahl.com/fileadmin/files/dew-stahl.com/documents/Publikationen/Werkstoffdatenblaetter/RSH/1.4404_de.pdf (accessed on 22 August 2023).
22. WHS Sondermetalle GmbH & Co. KG. Datenblatt Niob (NB, NbZr1). Available online: https://www.whs-sondermetalle.de/images/pdf/Nb-Niob.pdf (accessed on 22 August 2023).
23. Ge, F.; Peng, B.; Oliveira, J.P.; Ke, W.; Teshome, F.B.; Li, Y.; Zeng, Z. Dissimilar Laser Welding of a NiTi Shape Memory Alloy to Ti2AlNb. *Metals* **2021**, *11*, 1578. https://doi.org/10.3390/met11101578.
24. Yang, J.; Yu, Z.; Li, Y.; Zhang, H.; Zhou, N. Laser welding/brazing of 5182 aluminium alloy to ZEK100 magnesium alloy using a nickel interlayer. *Sci. Technol. Weld. Join.* **2018**, *23*, 543–550. https://doi.org/10.1080/13621718.2018.1425182.